Article

Design and Analysis of a Silicon-Based Pattern Reconfigurable Antenna Employing an Active Element Pattern Method

Ke Han, Zhongliang Deng and Xubing Guo *

School of Electronic Engineering, Beijing University of Posts and Telecommunications, Beijing 100876, China; hanke@bupt.edu.cn (K.H.); dengzl@bupt.edu.cn (Z.D.)
* Correspondence: gxb@bupt.edu.cn; Tel.: +86-10-6119-8559

Abstract: In this paper, a silicon-based radio frequency micro-electromechanical systems (RF MEMS) pattern reconfigurable antenna for a Ka-band application was designed, analyzed, fabricated, and measured. The proposed antenna can steer the beam among three radiating patterns (with main lobe directions of $-20°$, $0°$, and $+20°$ approximately) at 35 GHz by switching RF MEMS operating modes. The antenna has a low profile with a small size of 3.7 mm $\times$ 4.4 mm $\times$ 0.4 mm, and consists of one driven patch, four parasitic patches, two assistant patches, and two RF MEMS switches. The active element pattern method integrated with signal flow diagram was employed to analyze the performances of the proposed antenna. Comparing the measured results with analytical and simulated ones, good agreements are obtained.

Keywords: silicon-based; RF MEMS pattern reconfigurable antenna; Ka-band; RF MEMS switch; active element pattern method

1. Introduction

Pattern reconfigurable antennas received considerable attention owing to its attractive performance, as they can switch radiating patterns while keeping other operating parameters unchanged, such as operating frequency and polarization. In spacecraft, satellite, and missile applications, antenna constraints include weight, size, cost, and aerodynamic profile. Thus, the implementation of a pattern reconfigurable antenna with a low profile can alleviate those constraints. To date, many pattern reconfigurable antennas [1–5] have been developed, and reconfigurable antennas are commonly implemented using variodes [6,7] and PIN diodes [1,2]. Compared with the variodes, PIN diodes, and other technologies, radio frequency (RF) micro-electromechanical systems (MEMS) switches possess many attractive advantages, such as high linearity, high quality factors, and almost no Please check the sections highlight in yellow in "the whole text" as we have made little modification. direct current (DC) power consumption [8]. Many reconfigurable antennas have been developed by employing MEMS switches [9–12]. However, most of those reconfigurable antennas operate at a low frequency and do not have process consistence, namely, the RF MEMS switches were mounted on circuitry after the antenna patch was implemented, instead of the integrated manufacture of the antenna patch and the RF MEMS switches. In addition, with the various superiorities such as a wide bandwidth, a compact device structure, and a high data throughput capacity, devices in a Ka-band have many advantages.

A pattern reconfigurable antenna that consisted of a driven patch (active element) and two assistant radiated patches (passive elements) was designed [6], but the proposed method to design and analyze the assistant patches was severely dependent on full-wave simulation, which is

time-consuming. A beam-steering antenna was designed in [1], and the antenna was comprised of active patch and passive patch elements, but the analysis of the passive patch elements was rough and had no quantified calculations. In [13] an antenna using parasitic coupling was designed, but the analysis of the parasitic coupling function was insufficient, and the antenna only had simulated results. The active element pattern method integrated with the signal flow diagram needs to be shown to be effective in analyzing the passive antenna patches (parasitic coupling) [14,15]. The active element pattern of an element is defined as its radiation pattern when all other elements terminate in matched loads [16], and an antenna can be fully described by the its active element pattern and scattering parameters. This method is employed to design and analyze the proposed RF MEMS pattern reconfigurable antenna in this study.

In this paper, a pattern reconfigurable antenna operating at 35 GHz is proposed by employing RF MEMS switches. By changing the two RF MEMS switches operating modes, the proposed antenna can switch among four different kinds of operating states and obtain three kinds of reconfigurable patterns (because two operating modes possess the same pattern). The proposed pattern reconfigurable antenna is analyzed using an active element pattern method and a signal flow diagram. Comparing the calculated and simulated results with the measured ones, good agreement is acquired.

This paper is divided into five sections: Section 2 illustrates the design of the pattern reconfigurable antenna, Section 3 analyzes the operating mechanism of the proposed pattern reconfigurable antenna, Section 4 displays the measurement and results, and Section 5 summarizes the paper.

2. Design of the Pattern Reconfigurable Antenna

2.1. Antenna Design

A pattern reconfigurable is designed and its structure is illustrated in Figure 1, the close-ups shown in Figure 1b are the RF MEMS switch and its DC actuating circuit. The geometry configurations of Figure 1a are shown in Table 1. The antenna consists of one rectangle driven patch radiator, four rectangle parasitic patches, two assistant patches, and two RF MEMS switches. The RF MEMS switch was terminated by a $\lambda_g/4$ sector open stub and a high resistivity bias line. Parastic patch 1 and 2 are used for extending the operating bandwidth. The proposed pattern reconfigurable antenna patches and RF MEMS switches were all fabricated on a high resistivity silicon substrate with a thickness of 400 μm and a dielectric constant of 11.9.
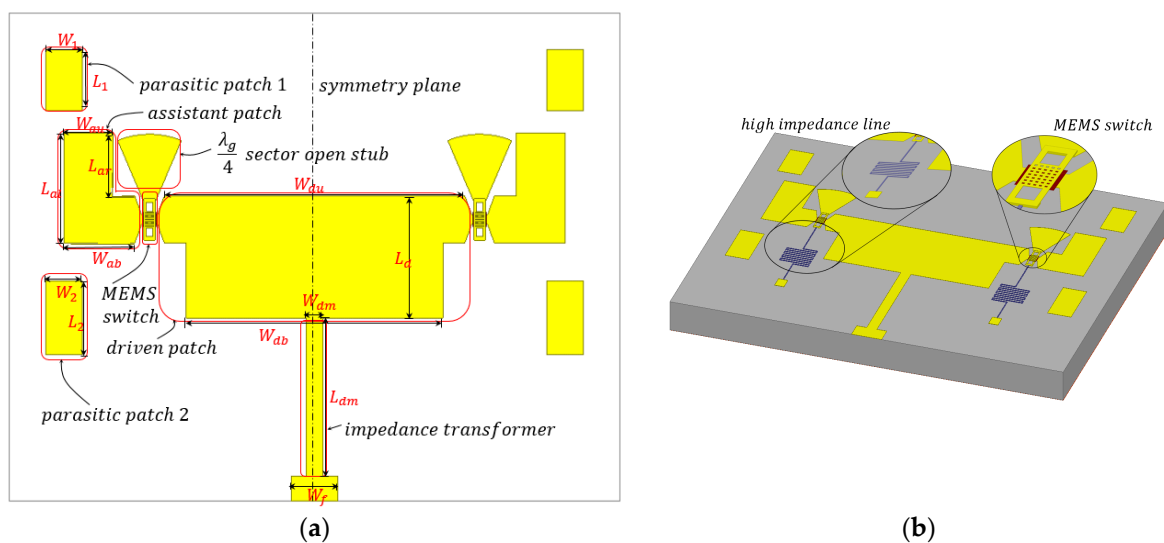

(**a**)　　　　　　　　　　　　　　　　　　　　　　(**b**)

Figure 1. Proposed pattern reconfigurable antenna. (**a**) The configuration of proposed antenna. (**b**) The 3D view of the proposed antenna.

Table 1. The geometry configuration of the proposed antenna.

Symbol	Value (µm)	Symbol	Value (µm)	Symbol	Value (µm)
W_{du}	2460	W_f	383	W_1	500
L_d	1000	W_{au}	400	L_1	300
W_{db}	2100	W_{ab}	580	W_2	600
W_{dm}	130	L_{al}	900	L_2	300
L_{dm}	1300	L_{ar}	518	-	-

By changing the mode of the RF MEMS switches, the antenna is capable of switching among four operating modes (00, 01, 10, 11; the "0" represents the up state, and the "1" stands for the down state) and achieving three pattern reconfigurable states in the *yoz* plane (φ = 90°) accordingly, because two of the operating modes are at the same pattern reconfigurable state. According to the measurement results of the fabricated pattern reconfigurable antenna, the three reconfigurable radiating patterns at operating frequency 35 GHz were obtained, i.e., left (approximately −20°), middle (approximately 0°), and right (approximately +20°), respectively. The detailed results of the reconfigurable radiating pattern main lobe direction and its associated RF MEMS switches operating modes are shown in Table 2.

Table 2. The reconfigurable radiating pattern main lobe direction and its associated radio frequency micro-electromechanical systems (RF MEMS) switches operating modes.

Mode	Description	Main Lobe Direction (φ = 90°)	Reconfigurable Radiating Pattern
(1,0)	Only left switch in the up state	θ = −20.2	left
(0,0)	Double switches in the up state	θ = −0.2	middle
(1,1)	Double switches in the down state	θ = −0.2	middle
(0,1)	Only right switch in the up state	θ = 20.5	right

2.2. RF MEMS Switch Design

The reconfigurations of the proposed antenna are realized by controlling the modes of RF MEMS switches; thus, the performance of RF MEMS switch is critical for the overall system. The thickness of the RF MEMS switch beam is 1 µm, and the air gap between the beam and the signal line that connects the derived patch and assistant patch is 1.5 µm. The other pivotal size is shown in Table 3. The top view and 3D view of the designed RF MEMS switch are illustrated in Figure 2.

Table 3. The pivotal size of the designed RF MEMS switch.

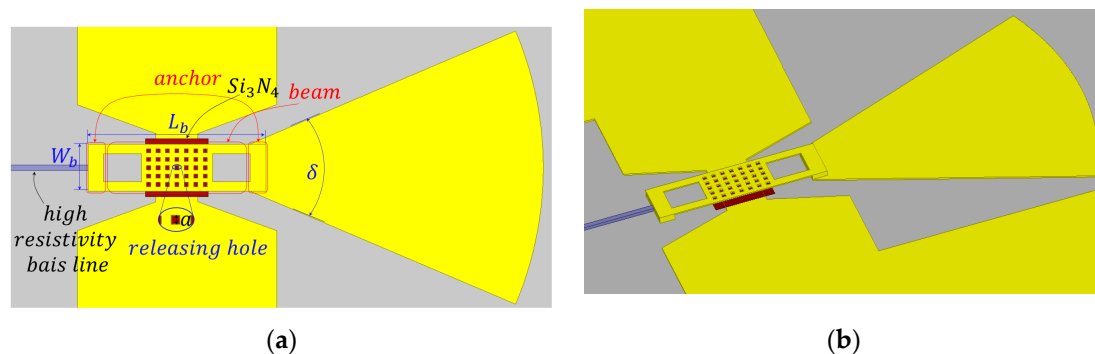| Symbol	Value	Symbol	Value	Symbol	Value	Symbol	Value
L_b	90 µm	W_b	340 µm	a	8 µm	δ	46°

Figure 2. Designed RF MEMS switch. (**a**) Top view. (**b**) 3D view.

As shown in Figure 2, the RF MEMS switch is terminated by a $\lambda_g/4$ sector open stub and a high resistivity bias line, which is used to apply the direct current. To alleviate the influences on return loss and resonant frequency, the $\lambda_g/4$ sector open stub is employed, which has many advantages such as miniaturization of struction and the convenience of connection. The dielectric shown in Figure 2a,b is Si_3N_4 with a thickness of 0.15 μm, and it is used to separate the beam and the signal line when the air gap is 0 μm. By actuating the RF MEMS switches using the direct current, the gap between the beam and the signal line varies from 0 to 1.5 μm (i.e., down state to up state). The down or up state determinate whether the assistant patch is connected to the driven patch, i.e., when the switch is in the down state (the gap is 0 μm), the assistant patch is detached from the driven patch, and vice versa.

According to the simulated results, the isolation of the proposed RF MEMS switch reaches 20 dB, and the insertion loss is 0.35 dB at operating frequency 35 GHz, respectively. The performance of the antenna can therefore be guaranteed. When the position of the RF MEMS switch beam is pulled to the point $(2/3)g_0$, the increase of the restoring force is exceeded by the increase of the electrostatic force. This leads to a rapid drop-down of the RF MEMS beam, and the actuating voltage reaches a maximum. The actuating voltage can be calculated by

$$V_p = \sqrt{\frac{2k_e}{\varepsilon_0 W_b L_d} \frac{g_0}{3} \left(\frac{2g_0}{3} + \frac{t_e}{\varepsilon_r}\right)^2} \tag{1}$$

where ε_0 is the dielectric constant of free space, ε_r is the relative dielectric constant of dielectric Si_3N_4, g_0 is the gap between the RF MEMS switch beam and the signal line, k_e is the elastic coefficient of the beam, t_e is the thickness of the beam, and W_b and L_d are the width and length of the beam, respectively. The actuating voltage is approximately 7.5 V calculated by Equation (1), but the measured voltage is actually 20.8 V. The measured actuating voltage is more than twice the calculated value, the main reasons for this phenomenon being the incomplete releasing of the polyimide and the inhomogeneity of the polyimide thickness. If the manufacture process has good release and flatness, the actuating voltage will be close to the theoretical value. The quality factor [8] of the RF MEMS switch is $Q = [4\varrho t_e^2 E^{-1/2}/\mu(W_b L_d)^2]g_0^3 \approx 1$. Thus, the pull in time of the RF MEMS switch is $ts \approx (27V_p^2)/(4\omega_0 QV_s^2) \approx 12.6$ μs, where E is Young's modulus, μ is the air viscosity coefficient between the RF MEMS beam and the Si_3N_4 dielectric, and Ω_0 is the mechanical resonant frequency, respectively.

3. Theory Analysis of Pattern Reconfigurations

An antenna array can be fully described by its scattering parameters and the active element pattern of each radiating element [16]. The proposed pattern reconfigurable antenna in this paper can be viewed as the degenerated antenna array shown in Figure 3a. (The whole structure of the reconfigurable antenna can be divided into three parts shown in Figure 3a, i.e., the left part, middle part, and right part. These three parts constitute an antenna array with three elements. However, the three elements in this array are not identical; both the left and right parts did not equip a separate microstrip feed line. Therefore, the reconfigurable antenna is equivalent to a degenerate antenna array.) Thus, the active element pattern, the scattering parameters, and the signal flow diagram method can be employed to analyze the proposed antenna appropriately. The active element pattern of an element is defined as its radiation pattern when all other elements are terminated in matched loads [16]. In this paper, a method combining an active element pattern and a signal flow diagram [17], is employed to analyze the pattern reconfigurations of the antenna-based RF MEMS switches.

The proposed antenna can be divided into three parts. As shown in Figure 3a, the driven patch and the feed line comprise Part 1, and Part 2 (namely load Z_2) consists of an assistant patch, a RF MEMS switch, parasitic patch 1, and parasitic patch 2, and the composition of Part 3 (namely load Z_3) is the same as Part 2. The parasitic patch in Part 2 and Part 3 are used to slightly tune the frequency of the overall antenna structure and extend the operating bandwidth. Without any loss of analysis

precision, the parasitic patches are involved in loads Z_2 and Z_3, as shown in Figure 3. Moreover, the port associated with each part is marked in Figure 3a as well.
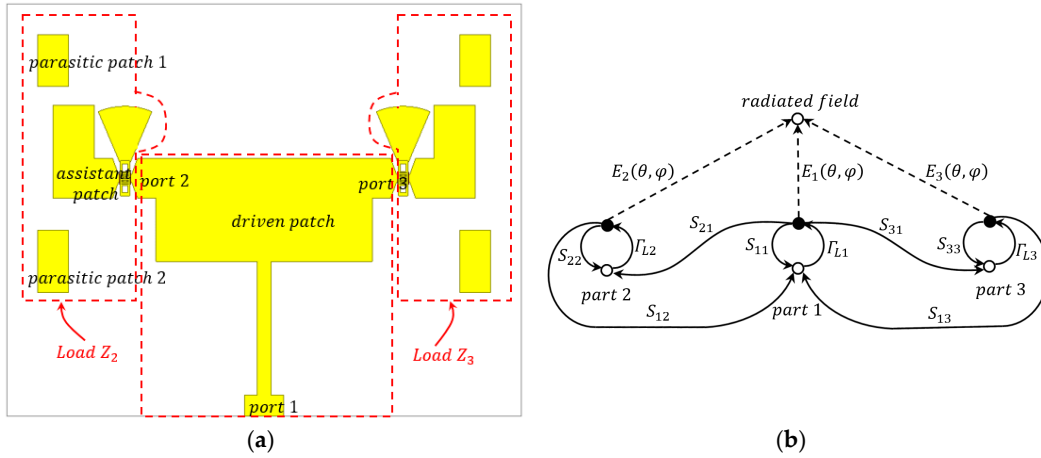

Figure 3. Divided parts of the antenna and its signal flow diagram. (**a**) Divided parts of the antenna. (**b**) Equivalent signal flow diagram of the proposed pattern reconfigurable antenna.

The proposed antenna can be modeled as an equivalent scattering parameter matrix S_D, which consists of a regular scattering parameter matrix S_r and the electric field intensity matrix E of active element pattern. The equivalent scattering parameter matrix S_D is defined as

$$S_D = \begin{pmatrix} S_r & E^T \\ E & 0 \end{pmatrix} \tag{2}$$

and the electric field intensity matrix E is

$$E = \begin{pmatrix} \mathbf{E}_1(\theta, \varphi) & \mathbf{E}_2(\theta, \varphi) & \mathbf{E}_3(\theta, \varphi) \end{pmatrix} \tag{3}$$

where $E_i(\theta, \varphi)$ is the electric field vector of each active element pattern, and E^T is the transpose matrix of E.

As shown in Figure 3, the driven patch (part 1) is terminated by load Z_2 and load Z_3. The regular scattering matrix S_r includes three ports, and S_{32} and S_{23} are all approximately equal to zero because the couplings between load Z_2 and load Z_3 can be neglected. According to the symmetry of the designed antenna overall structure, $S_{13} = S_{12}$ and $S_{31} = S_{21}$, respectively. Thus, S_r is defined as

$$S_r = \begin{pmatrix} S_{11} & S_{12} & S_{12} \\ S_{21} & S_{22} & 0 \\ S_{21} & 0 & S_{33} \end{pmatrix}. \tag{4}$$

The signal flow diagram of the proposed antenna is shown in Figure 3b, all of those parameters are extracted from a full wave simulation. The Γ_i is the reflection coefficient of Port No. *i*. Using the active element pattern and Mason rules, the return loss *RL* and gain $G(\theta, \varphi)$ of the proposed antenna are calculated as follows:

$$RL = 20 \log\left(\frac{M}{P}\right) \tag{5}$$

$$G(\theta, \varphi) = 20 \log \frac{N}{P\sqrt{\sum_{n=1}^{3} \left|I_n e^{j\varphi_n}\right|^2}} \tag{6}$$

where $I_n e^{j\varphi_n}$ is the signal current applied to Ports n, M, N, and P, which are defined as follows:

$$\begin{cases} M = S_{11} - S_{11}\Gamma_{L2}S_{22} - S_{11}\Gamma_{L3}S_{33} \\ +S_{11}\Gamma_{L2}S_{22}\Gamma_{L3}S_{33} + S_{12}^2\Gamma_{L2} - S_{12}^2\Gamma_{L2}\Gamma_{L3}S_{33} \\ +S_{13}^2\Gamma_{L3} - S_{13}^2\Gamma_{L2}\Gamma_{L3}S_{22} \\ \\ N = E_1(\theta,\varphi)(1 - \Gamma_{L2}S_{22} - \Gamma_{L3}S_{33} + \Gamma_{L3}S_{33}\Gamma_{L2}S_{22}) \\ +E_2(\theta,\varphi)S_{12}\Gamma_{L2}(1 - \Gamma_{L3}S_{33}) \\ +E_3(\theta,\varphi)S_{13}\Gamma_{L3}(1 - \Gamma_{L2}S_{22}) \\ \\ P = 1 + S_{11}\Gamma_{L1}[\Gamma_{L3}S_{33} + \Gamma_{L2}S_{22} - \Gamma_{L2}S_{22}\Gamma_{L3}S_{33}] + \Gamma_{L2}S_{22}\Gamma_{L3}S_{33} \\ -\Gamma_{L2}S_{12}^2\Gamma_{L1} - \Gamma_{L3}S_{13}^2\Gamma_{L1} - S_{12}^2\Gamma_{L2}\Gamma_{L3}S_{13}\Gamma_{L1} \\ -\Gamma_{L2}S_{22} - \Gamma_{L3}S_{33} + S_{13}^2\Gamma_{L3}\Gamma_{L1}\Gamma_{L2}S_{22} + S_{12}^2\Gamma_{L2}\Gamma_{L1}\Gamma_{L3}S_{33} \end{cases} \quad . \tag{7}$$

The Γ_i (i = 1, 2, 3) is the reflection coefficient of each port, which is given by

$$\Gamma_i = \frac{Z_{L,i} - Z_{0,i}}{Z_{L,i} + Z_{0,i}} \tag{8}$$

where $Z_{L,i}$ (i = 1, 2, 3) is the load impedance of each port, and $Z_{0,i}$ (i = 1, 2, 3) is the characteristic impedance of each port. In this paper, the impedance of Port 1 is matched, i.e., 50 Ω. Therefore, $\Gamma_1 = 0$. $Z_{L,2}$ and $Z_{L,3}$ are Z_2 and Z_3, as shown in Figure 3a, respectively. The characteristic impedance of Port 2 or Port 3 is equal to 87.5 Ω.

The simulation results show that the input impedance of Port 2 or Port 3 is always inductive and the real part of the input impedance is so small that it can been neglected. The return loss and the gain at $\phi = 90°$, $\theta = -20°$ of the proposed pattern reconfigurable antenna are shown in the contour maps (Figure 4a,b, respectively). In Figure 4, the horizontal axis and the vertical axis are the reactance value of load Z_2 and load Z_3. In order to alleviate the contradiction between the return loss and the gain, the two points in Figure 4 are selected to reconfigure the radiation pattern of the proposed antenna. In these two points, the return loss of the proposed antenna is approximately 10 dB, and the gain reaches approximately 5 dB.
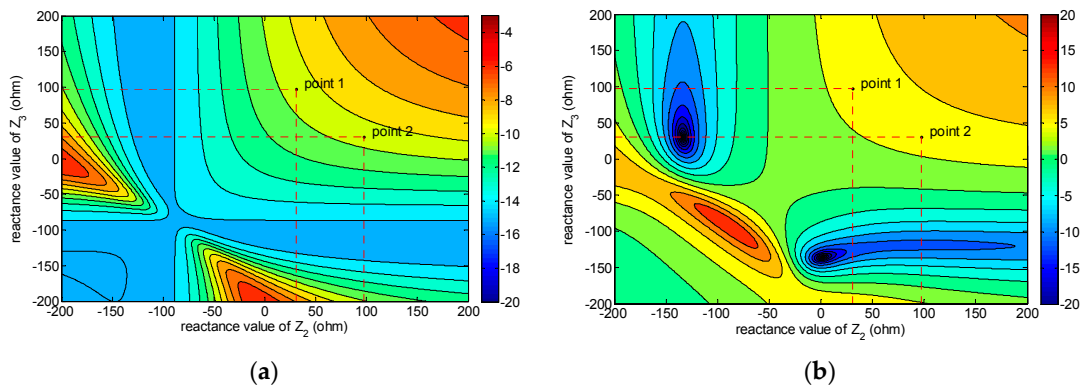

Figure 4. The return loss and gain distribution versus Z_2 and Z_3. (**a**) Return loss. (**b**) Gain at $\phi = 90°$, $\theta = -20°$ (The horizontal axis and the vertical axis are the reactance value of load Z_2 and load Z_3).

The value of load Z_2 and Z_3 can be reconfigured among Point 1 and Point 2 shown in Figure 4 by changing the operating modes. Each RF MEMS switch has two states, i.e., an up state (0) and a down state (1). The input impedance of the Part 2/Part 3 is (0.0808 + j1.1140) × 87.5 Ω ≈ (7 + j98) Ω in the "0" state, and (0.05 + j0.3503) × 87.5 Ω ≈ (4 + j31) Ω in the "1" state according to the simulated results, the value of the 87.5 Ω is the characteristic impedance of the port. Thus, the load conditions of the driven patch have four kinds of combination, as shown in Table 4. Fortunately, if the real part of the

input impedance (in RF MEMS switch "0" or "1" states) is neglected, the reactance value of the two points in Figure 4 will be reached by changing the RF MEMS switch operating modes among (1,0) and (0,1), i.e., Point 1 corresponding to RF MEMS switch state (1,0) and Point 2 corresponding to (0,1). Therefore, the main lobe direction of the proposed pattern reconfigurable antenna can be steered by changing the RF MEMS switch operating modes. The simulated gain results of the proposed RF MEMS pattern reconfigurable antenna are shown in Figure 5.

Table 4. The four kinds of combination for driven patch load conditions.

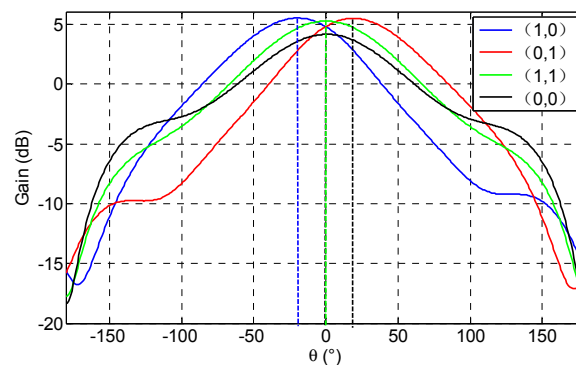| Switch State	(0,0)	(0,1)	(1,0)	(1,1)
(Z_2, Z_3) Ω	$(j98, j98)$	$(j97.5, j30.7)$	$(j30.7, j97.5)$	$(j30.7, j30.7)$

Figure 5. The simulated gain results of the proposed RF MEMS pattern reconfigurable antenna.

4. Fabrication, Measurement, and Results

4.1. Fabrication

The overall structure of the proposed pattern reconfigurable antenna and RF MEMS switches was fabricated on a high resistivity silicon substrate with a thickness of 400 μm and a dielectric constant of 11.9. The SiO_2 layer, which acts as an insulating layer, with a thickness of 0.3 μm is formed by thermal oxidation. Then, a 0.2-μm-thick layer of Al is deposited and patterned to define DC bias pads afterward and to form coplanar waveguide (CPW) transmission lines. Next, thin SiAl (approximately 0.05 μm) is patterned by lifting off to form the bias lines after deposition. A Si_3N_4 layer with a thickness of 1500 Å is patterned on the top of the electrode and bias lines by a plasma-enhanced chemical vapor deposition (PECVD) process. A 1.5-μm-thick layer of Al, which acts as an anchor, is evaporated. Polyimide as the sacrificial layer was cut down by a chemical mechanical polishing (CMP) process. The beam uses 0.6 μm of SiAl. Finally, the wafer is released in a plasma dryer to avoid the collapse of the membrane. The photographs of the proposed antenna and its close-up are shown in Figure 6.
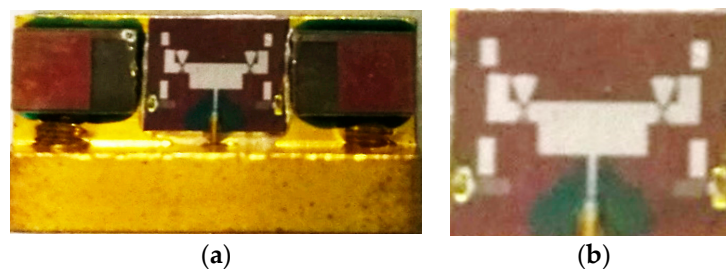

(**a**)　　　　　　　　　　　　　　　　　(**b**)

Figure 6. The photograph of the proposed pattern reconfigurable antenna taken by a microscope. (**a**) The antenna with testing holder. (**b**) Close-up of the antenna.

4.2. Measurement and Results

Input impedance of all operating modes at the desired frequency of 35 GHz is essential. The return loss of the proposed antenna was measured with the network analyzer Agilent PAN N5442A. The antenna was fed with a 50 Ω microstrip line, and the input impedance of the antenna was transformed by a transformer. The measured return losses of all modes were approximately 10 dB at the desired frequency of 35 GHz, as shown in Figure 7. Thus, the manufactured antenna has acceptable return loss performance.
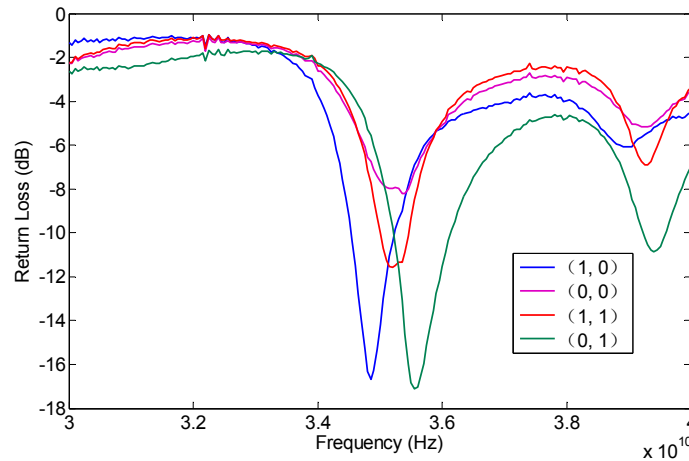

Figure 7. The measured return loss of the proposed pattern reconfigurable antenna in all states of the RF MEMS switches.

The radiating patterns of the proposed antenna are measured in the microwave chamber. As shown in Figure 8, the proposed pattern reconfigurable antenna can switch the radiating pattern among four operating modes by changing two RF MEMS switches states, and it can obtain three reconfigurable radiating patterns, i.e., left (approximately $-20°$), middle (approximately $0°$), and right (approximately $20°$), respectively.
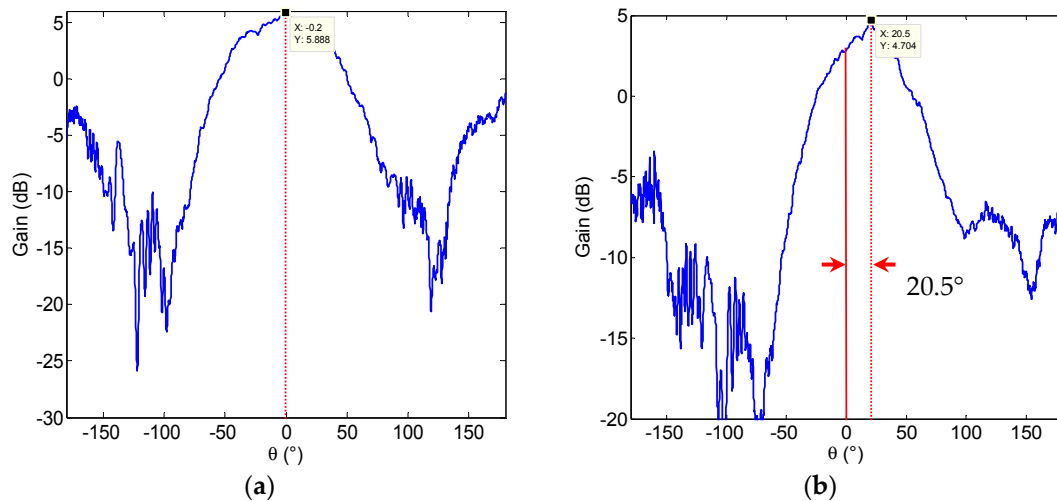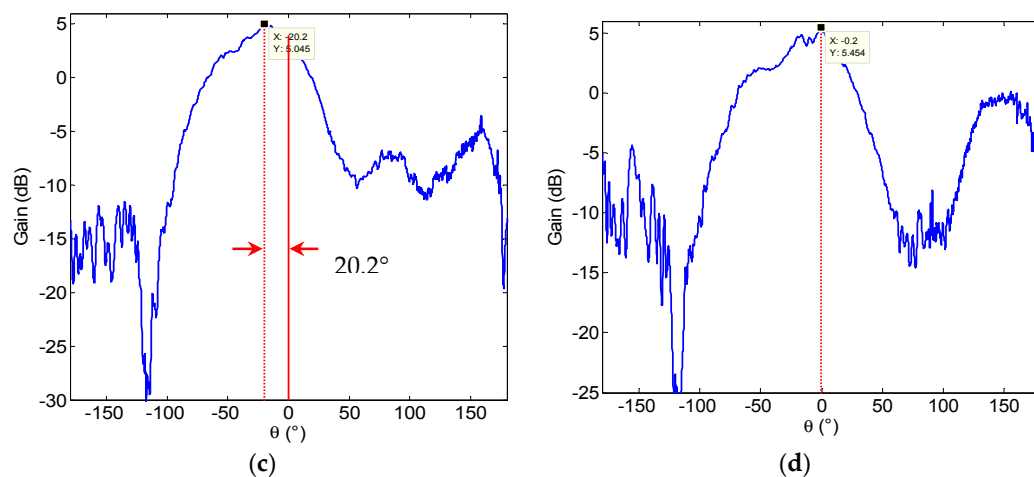

(a)

(b)

Figure 8. *Cont*.

Figure 8. The measured pattern of the proposed antenna using RF MEMS switches. (**a**) In the (0,0) state. (**b**) In the (0,1) state. (**c**) In the (1,0) state. (**d**) In the (1,1) state.

Comparing the measured results, the calculated results, and the simulated results shown in Figures 4 and 5, good agreement is achieved. The measured results in Figure 8 have a back lobe because of the coupling between the antenna patches and the testing holder. The error in fabrication, such as the resolution of lithography, the residual polyimide, the thickness inhomogeneity, the asymmetry between the left RF MEMS switch and the right RF MEMS switch, and the conductor loss are the other primary causes for the discrepancies observed in the measurements. If the manufacturing process is high quality, these discrepancies will be alleviated.

A comparison between the proposed pattern reconfigurable antenna and the available literatures was made, and the comparison results are shown in Table 5. The proposed antenna possesses a compact architecture structure and an acceptable reconfigurable angle range. It can be applied to a 5th-generation (5G) mobile communication and satellite communication system.

Table 5. Performance comparison of the proposed pattern reconfigurable antenna with the literature.

Available Literatures	[4]	[5]	[2]	[18]	This Study
Reconfigurable means	MEMS switches	MEMS switches	PIN diodes	Tunable Graphene Superstrate	MEMS switches
Antenna type	patch	slot-array	Double Layer patch	Double Layer	patch
Operating frequency (GHz)	34.8	30	27.5	30	35
Reconfigurable angles (°)	60	13	45	About 30	40
Block volume (mm³)	About $500 \times 500 \times 2$	About $7.112 \times 3.556 \times 40$	$5.1 \times 5.1 \times 1.274$	$16 \times 16 \times 10.3$	$3.7 \times 4.4 \times 0.4$

5. Conclusions

This paper proposes a pattern reconfigurable antenna by employing two RF MEMS switches. By changing the two RF MEMS operating modes, the proposed antenna can switch among three kinds of reconfigurable patterns, namely middle (approximately $0°$), left (approximately $-20°$), and right (approximately $20°$). The proposed pattern reconfigurable antenna was analyzed using an active element pattern method and a signal flow diagram. Comparing the measured results with the calculated and simulated results, good agreement was obtained. The proposed pattern reconfigurable antenna can be applied to a 5th-generation (5G) mobile communication and satellite communication system because of its excellent performance.

Author Contributions: Ke Han and Zhongliang Deng are the project manager; Xubing Guo conceived, designed and performed the experiments; Xubing Guo wrote the paper.

Conflicts of Interest: The authors declare no conflict of interest.

References

1. Park, Z.; Lin, J. A beam-steering broadband microstrip antenna for noncontact vital sign detection. *IEEE Antennas Wirel. Propag. Lett.* **2011**, *10*, 235–238. [CrossRef]

2. Palma, L.D.; Clemente, A.; Dussopt, L.; Sauleau, R.; Potier, P.; Pouliguen, P. 1-bit reconfigurable unit cell for Ka-band transmitarrays. *IEEE Antennas Wirel. Propag. Lett.* **2016**, *15*, 560–563. [CrossRef]

3. Ayoub, F.N.; Tawk, Y.; Woehrle, C.; Costantine, J.; Christodoulou, C.G. Reconfigurable cyclical patch antenna. In Proceedings of the 2015 IEEE International Symposium on Antennas and Propagation & USNC/URSI National Radio Science Meeting, Vancouver, BC, Canada, 19–24 July 2015; pp. 2249–2250.

4. Ratajczak, P.; Brachat, P.; Fargeas, J.M.; Baracco, J.M.; Toso, G. C-band and Ka-band reconfigurable planar reflectors. In Proceedings of the 2012 6th European Conference on Antennas and Propagation (EUCAP), Prague, Czech Republic, 26–30 March 2012; pp. 2618–2622.

5. Sánchez-Escuderos, D.; Ferrando-Bataller, M.; Baquero-Escudero, M.; Herranz-Herruzo, J.I. Pattern reconfigurable Ka-band slot-array antenna using RF-MEMS. In Proceedings of the 2010 IEEE Antennas and Propagation Society International Symposium, Toronto, ON, Canada, 11–17 July 2010; pp. 1–4.

6. Luther, J.J.; Ebadi, S.; Gong, X. Single-layer design of microstrip patch Electrically-Steerable Parasitic Array Radiator (ESPAR) with integrated DC isolation. In Proceedings of the 2012 IEEE MTT-S International Conference on Microwave Symposium Digest (MTT), Montreal, QC, Canada, 17–22 June 2012; pp. 1–3.

7. Luther, J.J.; Ebadi, S.; Gong, X. A low-cost 2 2 planar array of three-element microstrip Electrically Steerable Parasitic Array Radiator (ESPAR) subcells. *IEEE Trans. Microw. Theory Tech.* **2014**, *62*, 2325–2336. [CrossRef]

8. Rebeiz, G.M. *RF MEMS: Theory, Design, and Technology*; John Wiley & Sons: Hoboken, NJ, USA, 2004.

9. Zhou, L.; Sharma, S.K.; Kassegne, S.K. Reconfigurable microstrip rectangular loop antennas using RF MEMS switches. *Microw. Opt. Technol. Lett.* **2008**, *50*, 252–256. [CrossRef]

10. Al-alaa, M.A.; Elsadek, H.A.; Abdallah, E.A.; Hashish, E.A. Pattern and frequency reconfigurable monopole disc antenna using PIN diodes and MEMS switches. *Microw. Opt. Technol. Lett.* **2014**, *56*, 187–195. [CrossRef]

11. Rajagopalan, H.; Kovitz, J.M.; Rahmat-Samii, Y. MEMS reconfigurable optimized e-shaped patch antenna design for cognitive radio. *IEEE Trans. Antennas Propag.* **2014**, *62*, 1056–1064. [CrossRef]

12. Kovitz, J.M.; Rajagopalan, H.; Rahmat-Samii, Y. Design and implementation of broadband MEMS RHCP/LHCP reconfigurable arrays using rotated E-shaped patch elements. *IEEE Trans. Antennas Propag.* **2015**, *63*, 2497–2507. [CrossRef]

13. Balakumaran, T.; Sasidharan, D. Design of Microstrip Patch Antenna Array Using Parasitic Coupling. Available online: http://research.ijcaonline.org/ncict2015/number1/ncict1540.pdf (accessed on 20 December 2016).

14. Petit, L.; Dussopt, L.; Laheurte, J.M. MEMS-switched parasitic-antenna array for radiation pattern diversity. *IEEE Trans. Antennas Propag.* **2006**, *54*, 2624–2631. [CrossRef]

15. Pozar, D.M. A relation between the active input impedance and the active element pattern of a phased array. *IEEE Trans. Antennas Propag.* **2003**, *51*, 2486–2489. [CrossRef]

16. Pozar, D.M. The active element pattern. *IEEE Trans. Antennas Propag.* **1994**, *42*, 1176–1178. [CrossRef]

17. Poussot, B.; Kannappan, K.; Lissorgues, G.; Laheurte, J.M.; Picon, O. MEMS-based reconfigurable antenna for Ka band applications. In Proceedings of the Second European Conference on Antennas and Propagation, Edinburgh, UK, 11–16 November 2007; pp. 1–4.

18. Zhang, Z.L.; Wu, B. Radiation pattern reconfigurable antenna using double layer tunable graphene superstrate. In Proceedings of the 2015 Asia-Pacific Microwave Conference (APMC), Nanjing, China, 6–9 December 2015; pp. 1–3.